Supernova neutrino detection in NOvA

The NOvA Collaboration

M. A. Acero[2] P. Adamson[12] G. Agam[19] L. Aliaga[12] T. Alion[40]
V. Allakhverdian[26] N. Anfimov[26] A. Antoshkin[26]
E. Arrieta-Diaz[28] L. Asquith[40] A. Aurisano[6] A. Back[24]
C. Backhouse[4,45] M. Baird[20,40,46] N. Balashov[26] P. Baldi[25]
B. A. Bambah[18] S. Bashar[44] K. Bays[4,19] S. Bending[45]
R. Bernstein[12] V. Bhatnagar[33] B. Bhuyan[14] J. Bian[25,31] J. Blair[16]
A. C. Booth[40] P. Bour[9] R. Bowles[20] C. Bromberg[29]
N. Buchanan[8] A. Butkevich[22] V. Bychkov[31] S. Calvez[8]
T. J. Carroll[43,49] E. Catano-Mur[24,48] S. Childress[12]
B. C. Choudhary[11] T. E. Coan[38] M. Colo[48] L. Corwin[37]
L. Cremonesi[45] G. S. Davies[32,20] P. F. Derwent[12] P. Ding[12]
Z. Djurcic[1] M. Dolce[44] D. Doyle[8] D. Dueñas Tonguino[6]
E. C. Dukes[46] P. Dung[43] H. Duyang[36] S. Edayath[7] R. Ehrlich[46]
M. Elkins[24] G. J. Feldman[15] P. Filip[23] W. Flanagan[10] J. Franc[9]
M. J. Frank[35] H. R. Gallagher[44] R. Gandrajula[29] F. Gao[34]
S. Germani[45] A. Giri[17] R. A. Gomes[13] M. C. Goodman[1]
V. Grichine[27] M. Groh[20] R. Group[46] B. Guo[36] A. Habig[30]
F. Hakl[21] A. Hall[46] J. Hartnell[40] R. Hatcher[12] A. Hatzikoutelis[42]
K. Heller[31] J. Hewes[6] A. Himmel[12] A. Holin[45] B. Howard[20]
J. Huang[43] J. Hylen[12] F. Jediny[9] C. Johnson[8] M. Judah[8]
I. Kakorin[26] D. Kalra[33] D. M. Kaplan[19] R. Keloth[7] O. Klimov[26]
L. W. Koerner[16] L. Kolupaeva[26] S. Kotelnikov[27] M. Kubu[9]
Ch. Kullenberg[26] A. Kumar[33] C. D. Kuruppu[36] V. Kus[9]
T. Lackey[20] K. Lang[43] L. Li[25] S. Lin[8] A. Lister[49] M. Lokajicek[23]
S. Luchuk[22] S. Magill[1] W. A. Mann[44] M. L. Marshak[31]
M. Martinez-Casales[24] V. Matveev[22] B. Mayes[40] D. P. Méndez[40]

M. D. Messier[20] H. Meyer[47] T. Miao[12] W. H. Miller[31]
S. R. Mishra[36] A. Mislivec[31] R. Mohanta[18] A. Moren[30]
A. Morozova[26] L. Mualem[4] M. Muether[47] S. Mufson[20]
K. Mulder[45] R. Murphy[20] J. Musser[20] D. Naples[34] N. Nayak[25]
J. K. Nelson[48] R. Nichol[45] G. Nikseresht[19] E. Niner[20,12]
A. Norman[12] A. Norrick[12] T. Nosek[5] A. Olshevskiy[26] T. Olson[44]
J. Paley[12] R. B. Patterson[4] G. Pawloski[31] O. Petrova[26] R. Petti[36]
R. K. Plunkett[12] F. Psihas[20,43] A. Rafique[1] V. Raj[4] B. Ramson[12]
B. Rebel[12,49] P. Rojas[8] V. Ryabov[27] O. Samoylov[26]
M. C. Sanchez[24,1] S. Sánchez Falero[24] I. S. Seong[25]
P. Shanahan[12] A. Sheshukov[26,*] P. Singh[11] V. Singh[3] E. Smith[20]
J. Smolik[9] P. Snopok[19] N. Solomey[47] A. Sousa[6] K. Soustruznik[5]
M. Strait[31] L. Suter[1,12] A. Sutton[46] C. Sweeney[45] R. L. Talaga[1]
B. Tapia Oregui[43] P. Tas[5] R. B. Thayyullathil[7] J. Thomas[45,49]
E. Tiras[24] D. Torbunov[31] J. Tripathi[33] A. Tsaris[12] Y. Torun[19]
J. Urheim[20] P. Vahle[48] Z. Vallari[4] J. Vasel[20] P. Vokac[9] T. Vrba[9]
M. Wallbank[6] T. K. Warburton[24] M. Wetstein[24]
D. Whittington[41,20] D. A. Wickremasinghe[12] S. G. Wojcicki[39]
J. Wolcott[44] A. Yallappa Dombara[41] K. Yonehara[12] S. Yu[1,19]
Y. Yu[19] S. Zadorozhnyy[22] J. Zalesak[23] Y. Zhang[40] R. Zwaska[12]

[1]Argonne National Laboratory, Argonne, Illinois 60439, USA

[2]Universidad del Atlantico, Carrera 30 No. 8-49, Puerto Colombia, Atlantico, Colombia

[3]Department of Physics, Institute of Science, Banaras Hindu University, Varanasi, 221 005, India

[4]California Institute of Technology, Pasadena, California 91125, USA

[5]Charles University, Faculty of Mathematics and Physics, Institute of Particle and Nuclear Physics, Prague, Czech Republic

[6]Department of Physics, University of Cincinnati, Cincinnati, Ohio 45221, USA

[7]Department of Physics, Cochin University of Science and Technology, Kochi 682 022, India

[8]Department of Physics, Colorado State University, Fort Collins, CO 80523-1875, USA

[9]Czech Technical University in Prague, Brehova 7, 115 19 Prague 1, Czech Republic

[10]University of Dallas, 1845 E Northgate Drive, Irving, Texas 75062 USA

[11]Department of Physics and Astrophysics, University of Delhi, Delhi 110007, India

[12]Fermi National Accelerator Laboratory, Batavia, Illinois 60510, USA

[13]Instituto de Física, Universidade Federal de Goiás, Goiânia, Goiás, 74690-900, Brazil

[14]Department of Physics, IIT Guwahati, Guwahati, 781 039, India

[15]Department of Physics, Harvard University, Cambridge, Massachusetts 02138, USA

[16]Department of Physics, University of Houston, Houston, Texas 77204, USA

[17]Department of Physics, IIT Hyderabad, Hyderabad, 502 205, India

[18]School of Physics, University of Hyderabad, Hyderabad, 500 046, India

[19]Illinois Institute of Technology, Chicago IL 60616, USA

[20]Indiana University, Bloomington, Indiana 47405, USA

[21]Institute of Computer Science, The Czech Academy of Sciences, 182 07 Prague, Czech Republic

[22]Institute for Nuclear Research of Russia, Academy of Sciences 7a, 60th October Anniversary prospect, Moscow 117312, Russia

[23]Institute of Physics, The Czech Academy of Sciences, 182 21 Prague, Czech Republic

[24]Department of Physics and Astronomy, Iowa State University, Ames, Iowa 50011, USA

[25]Department of Physics and Astronomy, University of California at Irvine, Irvine, California 92697, USA

[26]Joint Institute for Nuclear Research, Dubna, Moscow region 141980, Russia

[27]Nuclear Physics and Astrophysics Division, Lebedev Physical Institute, Leninsky Prospect 53, 119991 Moscow, Russia

[28]Universidad del Magdalena, Carrera 32 No 22 – 08 Santa Marta, Colombia

[29]Department of Physics and Astronomy, Michigan State University, East Lansing, Michigan 48824, USA

[30]Department of Physics and Astronomy, University of Minnesota Duluth, Duluth, Minnesota 55812, USA

[31]School of Physics and Astronomy, University of Minnesota Twin Cities, Minneapolis, Minnesota 55455, USA

[32]University of Mississippi, University, Mississippi 38677, USA

[33]Department of Physics, Panjab University, Chandigarh, 160 014, India

[34]Department of Physics, University of Pittsburgh, Pittsburgh, Pennsylvania 15260, USA

[35]Department of Physics, University of South Alabama, Mobile, Alabama 36688, USA

[36]Department of Physics and Astronomy, University of South Carolina, Columbia, South Carolina 29208, USA

[37]South Dakota School of Mines and Technology, Rapid City, South Dakota 57701, USA

[38]Department of Physics, Southern Methodist University, Dallas, Texas 75275, USA

[39]Department of Physics, Stanford University, Stanford, California 94305, USA

[40]Department of Physics and Astronomy, University of Sussex, Falmer, Brighton BN1 9QH, United Kingdom

[41]Department of Physics, Syracuse University, Syracuse NY 13210, USA

[42]Department of Physics and Astronomy, University of Tennessee, Knoxville, Tennessee 37996, USA

[43]Department of Physics, University of Texas at Austin, Austin, Texas 78712, USA

[44]Department of Physics and Astronomy, Tufts University, Medford, Massachusetts 02155, USA

[45]Physics and Astronomy Dept., University College London, Gower Street, London WC1E 6BT, United Kingdom

[46]Department of Physics, University of Virginia, Charlottesville, Virginia 22904, USA

[47]Department of Mathematics, Statistics, and Physics, Wichita State University, Wichita, Kansas 67206, USA

[48]Department of Physics, William & Mary, Williamsburg, Virginia 23187, USA

[49]Department of Physics, University of Wisconsin-Madison, Madison, Wisconsin 53706, USA

 *Corresponding Author: andrey.sheshukov@jinr.ru

Abstract. The NOvA long-baseline neutrino experiment uses a pair of large, segmented, liquid-scintillator calorimeters to study neutrino oscillations, using GeV-scale neutrinos from the Fermilab NuMI beam. These detectors are also sensitive to the flux of neutrinos which are emitted during a core-collapse supernova through inverse beta decay interactions on carbon at energies of $\mathcal{O}(10 \text{ MeV})$. This signature provides a means to study the dominant mode of energy release for a core-collapse supernova occurring in our galaxy. We describe the data-driven software trigger system developed and employed by the NOvA experiment to identify and record neutrino data from nearby galactic supernovae. This technique has been used by NOvA to self-trigger on potential core-collapse supernovae in our galaxy, with an estimated sensitivity reaching out to 10 kpc distance while achieving a detection efficiency of 23% to 49% for supernovae from progenitor stars with masses of $9.6 \, \text{M}_\odot$ to $27 \, \text{M}_\odot$, respectively.

Contents

1   Introduction

The modeling and understanding of the stellar dynamics involved in core-collapse supernovae (SN) events require knowledge of the complex interplay between different physics processes which transition rapidly during the initial collapse of the star and the explosive expansion phases of the event. The neutrino burst that drives this explosive phase has been observed in the SN1987a event [1–4], but detailed measurement of the neutrino energy spectrum and time evolution of the neutrino flux are central to our understanding of these processes and will allow for more detailed models of the stellar dynamics to be evaluated.

The NOvA data acquisition system has been designed to detect and trigger on the time evolution of the rates of low energy interactions within the detectors. These interaction rates are compared, as part of the triggering, to the corresponding low energy interaction rates that are expected from models of a core-collapse supernova in our galaxy. This triggering process allows the NOvA experiment to capture both the energy spectrum and time evolution of the neutrino flux, contributing to the world's dataset on the dynamics of supernovae.

These trigger-level identification decisions allow data to be saved from each detector's data acquisition system's memory buffers to permanent storage for later offline analysis. The trigger decisions are also designed to be sent as alerts to the Supernova Early Warning System (SNEWS) [5] coincidence network where they can be combined with alerts and observations from other neutrino experiments worldwide. Because the expected rate of nearby supernovae is estimated at only a few per century, the trigger we present has been specifically tuned to preserve signal triggering efficiency at the cost of a higher rate of false positive trigger events. The trigger presented here, tuned to detector performance data, is projected to have an average false positive rate, for the NOvA Far Detector operating on the surface with minimal shielding and overburden, based on Poisson fluctuations of noise and cosmic ray induced activity, of one event per 7 days.

This trigger chain is discussed in the section 1.1 that follows. Section 2 describes the newly developed supernova flux generation scheme required to propagate the model dependent energy and time structure of neutrino interactions into the full detector response simulation. Section 3 then describes how data collected by the detectors are filtered and reconstructed in real time to suppress known backgrounds and identify potential low energy neutrino interactions. The methodology and implementation of the supernova trigger system within the NOvA detectors' readout and data acquisition system are presented in Sec. 4. Details of the system's performance and resulting detection sensitivities are reported and summarized in Sec. 5. The results and statistics of the trigger performance during the commissioning period are presented in Sec. 6.

1.1   NOvA Detectors

NOvA is a long-baseline neutrino oscillation experiment [6] using a pair of functionally identical liquid scintillator calorimeters to study electron neutrino appearance in the primarily muon neutrino NuMI beam [7] with a central energy of 2 GeV. The 14 kt Far Detector (FD) is located on the surface at the Ash River site in northern Minnesota, USA and is shielded by a concrete roof topped by an additional 15 cm of barite stone. The 810 km baseline for the neutrino oscillation measurements is determined by the separation between this site and the beam source. The approximately 300 t Near Detector (ND) is situated 100 m underground at Fermilab, 1 km from the beam source. Both detectors are comprised of planes of extruded polyvinyl chloride (PVC) composed of a custom formulation with titanium dioxide to increase

reflectivity [8]. Each extrusion panel is segmented into 3.9 cm by 6.6 cm detection cells. The lengths of these detection cells are 15.5 m for the Far Detector, while the shorter Near Detector cells are 3.9 m long. The detector planes are constructed from these extruded panels resulting in 384 cell wide planes (FD) or 96 cell wide planes (ND). Each cell is filled with a mineral oil based liquid scintillator [9], resulting in a 63% active mass fraction. The planes are alternated between a vertical (X-measuring) and horizontal (Y-measuring) orientation, with the Z-axis taken to be orthogonal to these planes and aligned with the beam direction. This orthogonal arrangement allows for simultaneous reconstruction of particle trajectories in the projected X/Z and Y/Z views as well as for three dimensional reconstruction through associative matching of hit information between readout views.

Scintillation light is collected and transported out of each cell via a loop of wavelength shifting fiber. This light is detected by an avalanche photodiode (APD) and the signal digitized by high speed readout electronics, providing both charge and time information for each of the 344,064 cells of the Far Detector at an effective continuous digitization rate of 2 MHz [10]. The resulting hit data is collated by the acquisition system's front-end readout electronics, and then transmitted to and buffered in the distributed memory of the experiment's trigger and buffer farm. This readout and buffer scheme provides circular style memory buffers which can be examined in real time to make triggering decisions or used by the final stages of event building to record portions of the data to permanent storage [10]. The same is done for the Near Detector, but the number of channels (20,192) is smaller and the effective sampling rate is larger (8 MHz).

The amplitude of the light signal is digitized in ADC counts, providing a measure of the energy deposited in the cell. For example, a muon crossing the center of a cell deposits about 10 MeV producing around 240 ADC counts in the Far Detector, or 530 ADC counts in the smaller Near Detector.

The raw data rate into the circular buffer systems averages $\sim$1.2 GB/s at the Far Detector under normal operating conditions. This rate is nearly constant and dominated by the more than 100 kHz rate of cosmic ray muons that penetrate the Far Detector overburden. This data stream is broken into 5 ms time windows, referred to as "milliblocks", which are stored in RAM buffers of a farm of commodity servers that are part of the Data Acquisition System (DAQ). The buffer farm has enough memory to store 1350 s of data. This results in the ability of the system to look backwards in time up to the depth of the buffer for identifying supernova signatures. The same methodology is used at the Near Detector, although its smaller size and larger overburden reduces the data rate to $\sim$13 MB/s and increases the buffer depth to 1900 s despite having fewer buffer nodes in the acquisition pool.

When the DAQ and trigger systems identifies a signature of interest, it designates a time window of data to record. The window is variable and can range from a minimum duration of 50 μs to the maximum duration corresponding to the size of the buffer. This data is retrieved from the buffers, collated, assembled into a custom data format, and written to disk for later analysis. Since the servers housing the buffer RAM also have significant CPU resources, the buffered data are examined asynchronously for patterns and topologies of interest. When a pattern or topology is identified, a trigger decision is issued which causes the corresponding data to be saved from the buffers to the NOvA data streams. This process of data-driven triggering is used to identify and record the elevated rates of small hit clusters that are indicative of a supernova neutrino burst, and has been operational since November 1, 2017.

1.2 Supernova neutrino signal

Core-collapse supernovae produce around 10^{58} neutrinos during the first seconds after the explosion. These neutrinos carry away about 99% of the gravitational binding energy released by the collapse and play a crucial role in the explosion mechanism of the star [11]. In particular, during the first 10 ms of the supernova, when the stellar core collapses to a neutron star, 1% of the total neutrino flux is produced as electron neutrinos due to the neutronization process. The enormous neutrino density interacts with the collapsing matter to power the shockwave that triggers the supernova explosion. This process is subsequently accompanied by an emission of neutrinos and anti-neutrinos of all flavors which are created through the pair-production channel. Because of their low interaction cross section, neutrinos can escape easily compared to more strongly interacting particles, which instead recycle their energy back into the hot dense medium of the proto-neutron star. These neutrino emissions serve as the dominant cooling mechanism for the proto-neutron star.

Modern models of core-collapse supernova explosions often feature complex 3D simulations of the processes during the core collapse. Results of these simulations predict various neutrino spectra and energy-luminance curves vs. time for different models that probe both astrophysics and neutrino parameters [12–14]. Aside from these subtleties, the basic features of the neutrino "light curve" are common to all models. The light curve exhibits an initial, short neutronization burst, then there is about a 1 second of neutrino emissions as the proto-neutron star accretes infalling matter and the shock front develops. This is followed by the emissions during exponential cooling, which occur over the next tens of seconds. The neutrinos, prior to any oscillation or collective effects, are produced in roughly equal populations with respect to lepton flavor. These populations have energy spectra in the tens of MeV, with slightly hotter spectra for the muon and tau neutrino species, cooler for electron anti-neutrinos, and the coolest for the electron neutrinos.

In this work we use the neutrino flux from the simulations by the Garching group [13]. This is done for two progenitor star masses of 9.6 and 27 solar masses (see Fig. 1), which the Garching group have chosen as representative of typical low- and high-mass supernovae. We do not consider the effects of neutrino oscillations or self-interactions in this work, for purposes of more straightforward comparisons to other detectors (as per Ref. [11]), although Sec. 5.1 describes their rough effect on the triggering. These effects, potentially leading to spectral distortions, "swapping", or "splits" (see Sec. 4 in [13]), could provide the opportunity to study the neutrino properties from an observed supernova neutrino signal. NOvA's sensitivities to such interesting physics will be the subject of a future paper.

1.3 Detection channels

The observation of the neutrino signal from a core-collapse supernova is highly dependent on the detector's technology and composition. In the case of a hydrocarbon based scintillator detector like those used in the NOvA experiment, the prominent channels for observation of neutrinos in the tens of MeV range are inverse beta decay (IBD), elastic scattering on electrons, and neutral current interactions on carbon (see Fig. 2). These signatures, as observable in NOvA, are described in the following subsections and summarized in Tab. 1, while other interaction channels produce few observable signals in the NOvA detectors.

1.3.1 Inverse beta decay (IBD)

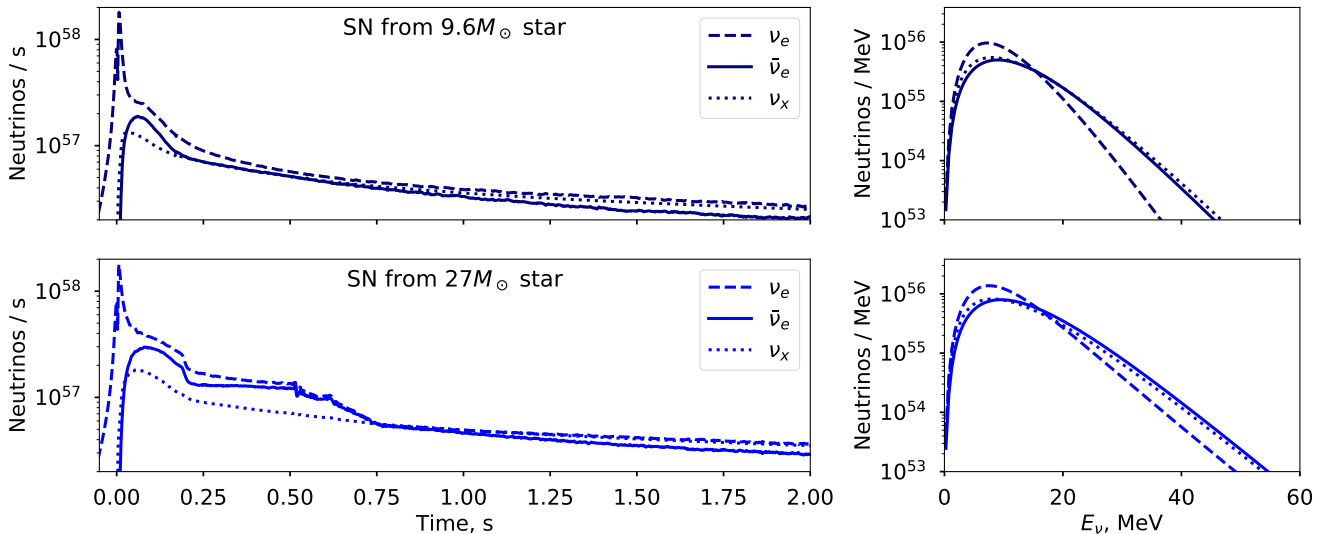$$\bar{\nu}_e + p \rightarrow e^+ + n$$

Figure 1. Expected neutrino production vs. time (left) and energy (right) from collapsing stars with a mass of $9.6\,\mathrm{M_\odot}$ (top) and $27\,\mathrm{M_\odot}$ (bottom), from the simulation by the Garching group [13]. This simulation does not include flavor changing effects such as neutrino oscillations and collective effects.

When an electron anti-neutrino interacts with a proton in the low-Z hydrocarbons which make up both the active and inactive regions of the NOvA detectors, it produces a positron and a low energy neutron. Both of these particles can propagate significant distances within the active regions of the detector and register as activity. To compute the IBD reaction rates in the NOvA detector, we use the IBD cross-section calculation by Strumia and Vissani [15, Table 1], as it applies specifically to supernova neutrino energies. This interaction channel is by far the dominant channel for supernova bursts that can be detected in the near and far NOvA detectors. In addition, there is a simple kinematic correlation between the energy of the incident anti-neutrino and the energy of the resulting positron, which is observed in the final state of the interaction. In this manner, the IBD channel allows for a computation of the neutrino energy spectrum from the positron kinetic energy E_{e+} via

$$E_{\bar{\nu}_e} \simeq E_{e+} + 1.29 \text{ MeV}. \tag{1.1}$$

1.3.2 Elastic scattering of neutrinos on electrons

$$\nu_x(\bar{\nu}_x) + e^- \to \nu_x(\bar{\nu}_x) + e^-$$

The process of elastic scattering of neutrinos on electrons is common to all (anti)neutrino flavors [16]. In the final state the scattered electron is observed. The observed amplitude for the process must be summed over the active neutrino and anti-neutrino species. However, the ν_e-electron scattering has the largest interaction cross section and is the dominant interaction mode for this process. In the NOvA detector, this results in a larger contribution to the observed activity coming from the ν_e channel as compared with the other five subdominant interaction channels. Unlike the IBD channel, this process preserves significant information on the directionality of the incident neutrino, which is carried through into the final state kinematics of the observed electron. However, in the case of the NOvA detector geometry,
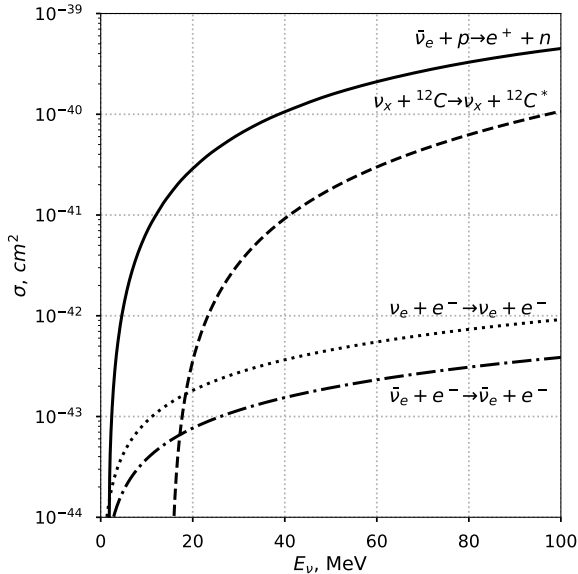
Figure 2. Cross section vs. energy for the neutrino interaction channels relevant for the NOvA detectors, from [15–17].

the resulting electrons are low enough in energy that their mean path length through the active detector mass when combined with the coarse $(3.9\,\text{cm} \times 6.6\,\text{cm})$ granularity of the NOvA readout cells is insufficient to reconstruct the incident neutrino angle with the precision needed to provide pointing information for the parent supernova. As a result, this channel is included in the supernova signal rate calculations, but no attempt is made to reconstruct neutrino directions from it.

1.3.3 Neutral current scattering on carbon

$$\nu_x(\bar{\nu}_x) + {}^{12}C \rightarrow \nu_x(\bar{\nu}_x) + {}^{12}C^*(15.1 \text{ MeV})$$

Neutral current neutrino interactions probe the full flavor content of the neutrino sector, permitting the ν_μ and ν_τ components of the supernova to be detected, unlike the corresponding charged current interactions which have interaction thresholds significantly above the modeled supernova neutrino energy spectra. In particular, neutral current interactions on carbon nuclei result in a nuclear excitation. The subsequent 15.1 MeV de-excitation photon [17] is observable as near-threshold activity in the NOvA detectors, with higher efficiency in the Near Detector with its shorter cells and consequent smaller light attenuation. While this process is subdominant compared to the elastic scattering and IBD channels, it does contribute to the overall rate and provides a mechanism to probe the interactions independent of lepton flavor.

2   Simulation chain

Monte Carlo simulations of supernova neutrino bursts are performed in order to understand how the resulting signal channels will register within the NOvA detectors. These simulations are produced using different models for the predicted supernova fluence, and the resulting predictions are then scaled by the distance to the supernova to understand the signal rates.

Table 1. Estimated average number of neutrino interactions in the NOvA detectors for dominant interaction and detection channels for Garching supernova neutrino flux simulations from $9.6\,M_\odot$ and $27\,M_\odot$ progenitor stars at a distance of $10\,\mathrm{kpc}$.

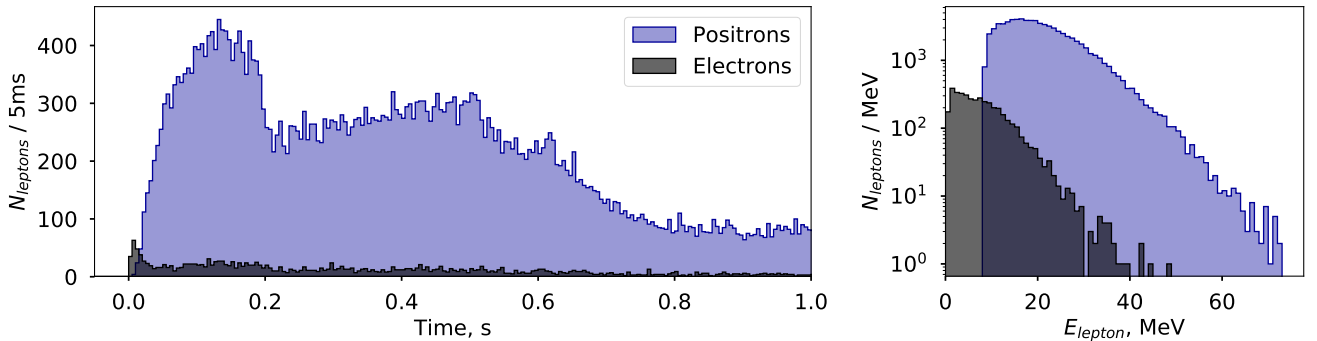| Interaction channel	Far Detector		Near Detector	
	$9.6\,M_\odot$	$27\,M_\odot$	$9.6\,M_\odot$	$27\,M_\odot$
Inverse beta decay	1593	3439	24	51
Elastic scattering on e^-	143	259	3	5
Neutral current on ^{12}C	67	166	1	3
Total	1803	3864	28	59

Figure 3. Results of GenieSNova simulation of SN neutrinos from a $27\,M_\odot$ progenitor star at $2\,\mathrm{kpc}$ distance, interacting in the NOvA Far Detector: time (left) and energy (right) distributions of secondary charged leptons. The electrons come from the neutrino-electron elastic scattering, and positrons are produced in the IBD process. The minimum neutrino energy for this simulation was set to $10\,\mathrm{MeV}$ to reduce the calculation time, which leads to a cutoff in the positron spectrum, seen on the right plot. This does not affect the NOvA result, as positrons below $10\,\mathrm{MeV}$ are not reconstructed by NOvA (see Fig. 9).

These fluences are convolved with the neutrino interaction cross sections on the NOvA detector materials to predict the expected interaction rates within the detector. This convolution is performed on an interaction-by-interaction basis so that detailed examination of the final state particles of each interaction can be propagated through the detector simulation. The detector simulation incorporates both detailed models both for the particle propagation through the media as well as for light yields and propagation of scintillation and Cherenkov light through the detector. The simulation also includes custom models of the NOvA electronics and digitization chain, which utilize measured detector responses and detector efficiencies. The combination of steps in this end-to-end simulation chain thus allows the computation of the detection efficiencies for the supernova signal channels, as well as the overall efficiencies for supernova trigger algorithms which operate on the ensemble of signal and background activity.

2.1 GenieSNova

For the NOvA supernova trigger, a dedicated software package named "GenieSNova" was developed to simulate interactions of supernova neutrinos inside the NOvA detectors. This

new package generates neutrinos according to a supernova neutrino flux distribution including both the time structure and energy distributions. It then then simulates neutrino interactions on the NOvA materials according to the detectors' geometry. The GenieSNova package interfaces models of supernova neutrino fluence from the Garching group [13] and the Supernova Neutrino Database [14] with the GENIE neutrino interactions generator [18] to accomplish this simulation.

The daughter particles from the interactions are then propagated through the detector with the Geant4 [19] based NOvA detector simulation [20] which is used throughout the NOvA experiment for both beam neutrino analysis and non-beam studies. This simulation chain allows for easy integration of the supernova analysis into the standard NOvA simulation pipelines and permits the use of standard NOvA reconstruction and analysis tools for clustering, tracking, and event reconstruction.

The development of GenieSNova was required to properly simulate the macroscopic time structure of the supernova neutrino signals under different model assumptions. The standard GENIE generator has been developed primarily for accelerator beam induced interactions and for atmospheric neutrino interactions. Both of these neutrino sources are not considered to have extended time correlations. In contrast, the supernova neutrino burst models required correlation of the neutrino generation across time scales on the order of tens of seconds. To develop a trigger which relies on the time structure of the burst, the ability to produce both time and energy dependent neutrino interactions had to be introduced to GENIE. In addition to the extended time structures, the GenieSNova simulation modified the NOvA interfaces to the underlying GENIE generator to allow for neutrino energies down to $1\,\mathrm{MeV}$ to be correctly propagated through the simulation infrastructure. This is in contrast to the nominal beam neutrino simulation that is used for the NOvA oscillation measurements which is tuned to efficiently handle neutrino interactions in the 1–$2\,\mathrm{GeV}$ regime.

In the simulation of the supernova event by the GenieSNova framework, we considered the visible signal in the NOvA detector to be dominated by inverse beta decay and elastic neutrino scattering on electrons channels. These two channels represent 96% of the total expected number of interactions for all interaction channels. The spectra of the outgoing leptons as a function of time and energy for these channels, as simulated through the GenieSNova simulation chain is shown in figure 3.

The carbon de-excitation and other delayed coincidence channels were not included in the simulation that was used to determine the trigger templates, due to model uncertainties and limitations in the detector readout structure. However, these channels and other subdominant processes, in the event of a real supernova event, would be fully recorded by the detector data stream and could be reconstructed in the offline data analysis framework. These channels may be included in future implementations of the triggering simulations to expand the trigger sensitivities by fully accounting for all expected visible activity in the detector volume.

2.2 Detector Simulation

Once GenieSNova has produced a time profile of supernova neutrino interactions and their daughter particles that would appear in a NOvA detector, the particles are fed to the same detector simulation used in the beam neutrino analyses. No modifications to the geometry are needed for the supernova signal and all standard calibrations are applied to the detector response as are applied in the beam neutrino oscillation analyses. This simulation includes the light yields of the NOvA liquid scintillator using a custom software package developed and

tuned to NOvA data and measurements of light yields made by the NOvA collaboration [9]. This tuning accounts for both scintillation light and Cherenkov light that is generated within the liquid and transported through the wavelength-shifting fiber optics. The propagated light is then fed to a model for the response of the NOvA avalanche photodiodes (APD) and a simulation of the readout electronics, digitization, digital signal processing, and readout chain. The results are formatted and stored in the same format as data from the physical detector systems, which allows the information to be subsequently used as input to the trigger decision system.

2.3   Background data overlays

The observable signals in both the IBD and elastic scattering channels have mean energies between 10 and 20 MeV, with single detector cell responses below 10 MeV. This places these signals close to the noise floor and zero suppression threshold for the digitization and readout electronics.

In order to accurately model detection algorithms, these signals need to be placed in the context of the expected cosmic ray induced activity and the electronics noise that is present on the front-end electronics. To accomplish this, "minimum bias" data is collected from the detector. The minimum bias data stream produces a sequence of complete 5 ms time windows of detector readout. These 5 ms windows are continuous and contiguous in time (*i.e.*, each 5 ms window contains all activity for that time window and sequential 5 ms windows in the data stream used for the supernova analysis are contiguous such that when combined they provide no temporal gaps in the readout). The window length of 5 ms is chosen to correspond to the size of the milliblock which is the data acquisition system's internal discretization of the continuous readout stream. This minimum bias data is considered to be free of supernova induced activity, and simulated supernova signal events are then overlaid on top of data to produce a data/Monte Carlo hybrid readout stream which represents the expected full detector response to a supernova event. This data stream is formatted identically to the actual detector data, but includes both the simulated signal and real backgrounds. These "overlay" files are then used to tune and test reconstruction and trigger algorithms and calculate signal selection efficiencies and purities.

3   Detection of neutrino interaction candidates

Each neutrino interaction channel under consideration results in an observable signal from a low energy electron, positron, or photon. Identifying these low energy signals is challenging in both the Near and Far NOvA detectors. Both detectors are optimized for calorimetry of GeV-scale electromagnetic showers, corresponding to the electron neutrino appearance topology from the 2 GeV NuMI neutrino beam [21]. These showers extend over distances of meters in the low-Z NOvA detectors and consist of tens of hits above the zero suppression cutoff[1], while IBD positrons from a supernova have detectable energies of 10–30 MeV. These particles induce far smaller signals, with only 1–4 hits being registered above the zero suppression threshold in the scintillator cells. This response to low energy particles is shown in the left of Fig. 4. In the NOvA detectors, this response is further suppressed by the attenuation of the scintillation light through the active medium and along the fiber optic path used for readout.

---

[1]The mean number of hits for a muon track arising from a ν_μ interaction reported in a NOvA detector is 122.
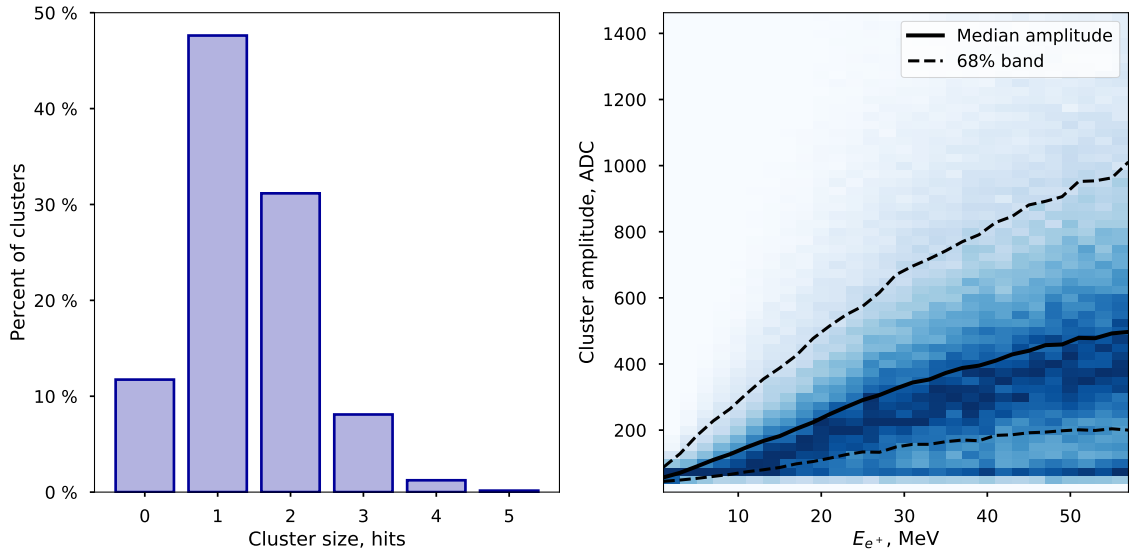
Figure 4. Distribution of the number of hits from simulation, produced by positrons from supernova neutrino IBD interactions in the NOvA Far Detector using 9.6 $M_\odot$ progenitor model (left), and their summary amplitude in ADC counts (right). The solid line shows median amplitude, and dashed lines show the 68% band of ADC vs positron energy.

Even weaker 8.6 MeV photon signals from IBD neutron capture on ^{35}Cl will also be present. Given the presence of a large background, such signals are difficult to match with the positron signal, due to their time and space separation. Therefore the IBD neutrons are not considered in this work.

3.1 Background rejection

The difficulty of detecting low energy interaction hit clusters is compounded by the rates of background activity in the NOvA detectors. In contrast to other supernova neutrino experiments currently operating [11], the NOvA detectors have considerably smaller overburdens with which to shield the detector volumes from sources of cosmic induced backgrounds.

The 300 t Near Detector has the larger overburden of the two detectors at 225 meters water equivalent (mwe). At this depth, the average cosmic ray rate results in 37 Hz of observed activity in the Near Detector. This rate is sufficiently low that it has minimal impact on the efficiency for identification of low energy hit clusters. In contrast, the Far Detector building is located on the surface, where the overburden is 3.6 mwe resulting in an observed average 148 kHz rate of cosmic ray muons, electromagnetic showers and other cosmogenically induced activity [22]. This activity comes from the direct passage of cosmic rays through the active volume of the detector, as well as from secondary neutrons, delta rays, spallation products, and Michel electrons from muon decay. The first step for a trigger trying to find low energy clusters consistent with neutrino interactions from a supernova is thus to remove hits from other physics processes or readout noise. The remaining hits can then be examined further.

3.1.1 Atmospheric muons

Michel electrons coming from decay of atmospheric muons with a kinematic upper edge at 53 MeV are of comparable energy to the IBD signal positrons from supernova neutrinos.

They form the primary source of background for the supernova signal, but can be suppressed through a process that associates a low energy cluster with the stopping muon track that is the parent of the Michel electron.

In this analysis, muon track trajectories are identified and reconstructed using a tracking algorithm based on the Hough transform [23]. Termination points for these trajectories that occur within the detectors' fiducial volumes are treated as the endpoint or stopping position for the muons. Hits associated with the muon track are removed from consideration. Additionally, hits separated from the track endpoint by less than 32 cm and delayed by no more than by 10 μs are considered to be produced by the Michel electron and rejected from the signal sample for the neutrino burst signature. Note that the same similarity between the spectra of SN induced IBD positrons and Michel electrons which makes them an important background to remove also allows us to benchmark our simulations, as Michel electrons are a standard calibration for NOvA.

3.1.2 High energy showers

Extensive air showers and other high energy activity induced by cosmic rays, including catastrophic bremsstrahlung interactions, can produce high hit multiplicities in the NOvA detector. Many of the clustering and tracking algorithms used for low energy event reconstruction are susceptible to failures under these conditions both in terms of physics content as well as in terms of algorithmic scaling behavior, as many of the clustering methods have $\mathcal{O}(n_{hits}^2)$ algorithm complexity. For this reason, high multiplicity time windows in the data are excluded from the trigger decisions. Time windows of 1.1 μs containing hits with a total amplitude exceeding 1,000,000 ADC for the Far Detector and 300,000 ADC for the Near Detector are excluded. In addition, a trailing exclusion window of 350 μs is imposed to allow the detector electronics to recover from known response effects related to high instantaneous rates. Remnant track segments are removed after this process by imposing a maximum size requirement on candidate positron clusters. This process is discussed in Sec. 3.2.

3.1.3 Electronics noise in readout channels

Zero suppression thresholds for the front-end electronics are set based on the measured noise envelopes produced by APDs and their corresponding amplification circuits. The noise profiles for the circuits are assumed to be approximately Gaussian, and as such the zero suppression threshold is set at $+4\sigma$ and $+5\sigma$ from the channel baseline for the Far and Near detectors respectively. At these suppression levels, the dark current and leakage current in the detection circuits produce single hits in the readout that are not correlated with particle trajectories or interactions in the detectors.

The APDs and front-end amplifier/digitization boards used in NOvA are sometimes subject to electrical failures which can cause individual channels to give either excessive or suppressed hit rates. Channels experiencing these failures are classified as degraded and excluded from the analysis. These electronics are replaced at regular maintenance intervals, resulting in an average dead fraction of 0.12% for Far Detector channels and 2.5% for Near Detector channels. To mitigate the effect of this loss prior to their replacements during maintenance, a map of the average hit rates on a per channel bases is calculated and used to mask off degraded channels. For the purposes of the supernova trigger system, channels are masked in the trigger software if they have an inactivity fraction exceeding 90% (cold channel) or have a single channel hit rate in excess of 1 kHz when averaged over a one hour period (hot channel). The activity map used to provide this channel masking is recalculated

Table 2. Average rejection of single hits from various background sources in the NOvA detectors: the first row is the total rate, then the effects of each cut follow, with the last row being the remaining rate of single hits. Low-rate events such as the high energy showers and Near Detector cosmics have a high variance, since very few time windows are affected quite strongly by such activity.

		Average hit rate, kHz	Fraction	Variation
Far Detector	Total detector hit rate	74971.09	100.00%	1.21%
	Hits from cosmic ray muons	16702.19	22.28%	5.06%
	Hits from Michel electrons	4727.62	6.31%	5.18%
	Single channel noise	1533.98	2.05%	2.04%
	High energy cosmic shower activity	96.26	0.13%	839.35%
	Activity after background suppression	56344.94	75.16%	0.89%
Near Detector	Total detector hit rate	715.14	100.00%	11.01%
	Hits from cosmic ray muons	2.57	0.36%	255.36%
	Hits from Michel electrons	1.14	0.16%	295.76%
	Single channel noise	445.88	61.90%	10.60%
	High energy cosmic shower activity	0.04	0.01%	8796.71%
	Activity after background suppression	269.89	37.74%	9.03%

hourly with the maps being archived in the trigger system. When a channel is tagged for exclusion, it remains excluded from the supernova trigger analysis until it is observed to respond within normal operational parameters for a period of 24 hours. It is then re-enabled in the subsequent hourly update to the trigger channel masks.

The effect of degraded channels (both hot and cold) on the detection of simulated signal is taken into account by applying the channel masks, obtained from the detector minimum-bias data. Due to the low fraction of excluded channels, the impact on the resulting efficiency of the supernova signal detection is small, compared to other background rejection procedures.

The total integrated rate of single channel noise after the background hits suppression across the 344,064 channels of the Far Detector is 56.3 MHz. This rate includes both instrumental noise and low-level light from the environment or sub-threshold particles. Cross-talk between adjacent channels can cause correlations in these rates which are able to mimic the low energy multi-hit clusters that are being searched for in the supernova analysis. However, the X-view and Y-view readout systems are electrically and spatially decoupled and there are no known couplings between the readouts of adjacent detector planes. As a result single-hit sources of noise are significantly suppressed by requiring a temporal coincidence between hits in adjacent planes. During the part of the clustering algorithm discussed in Sec. 3.2, a temporal coincidence of less than 32 ns is required for a candidate cluster to be formed. At this level of matching, the total noise rate is further suppressed by a factor of 240 from 56.3 MHz to 232 kHz.

The effectiveness of the selection requirements employed to reduce contributions to the single hit rate from atmospheric muons ($\sim$100 kHz at the Far Detctor, $\sim$30 Hz at the Near), high energy showers ($\sim$5 Hz at the Far Detector), and electronic noise are summarized in Tab. 2. These are drawn from a typical one minute time period of minimum bias data in the detectors, showing the background rates close to the average level. The milliblock-to-milliblock variation for high-rate backgrounds is quite steady. Comparatively rare backgrounds which strongly affect few milliblocks have high variance.

3.2 Clustering algorithm

The hits remaining after the removal of background activity, as summarized in Tab. 2, potentially belong to low energy neutrino interactions. The identification of these interactions requires a multi-stage process of hit clustering and pattern recognition which form the interaction candidates. The first set of clustering algorithms uses the timing information associated with each hit in the NOvA detector. Single-hit timing in the NOvA detectors is determined by fitting and interpolating the waveform data that is acquired from the front-end digitizers to the idealized shaper circuit response function of the amplifier circuit. The process uses a set of four samples separated by 500 ns at the Far Detector (135 ns at the Near) to determine the rising edge of the response pulse and the time, t_0, of the activity that caused the light. This process results in a single-hit timing resolution of 8–12 ns. This allows for a simple clustering algorithm to be applied based on temporal activity. Cosmic ray muons are easily identified using this method, as $\beta \approx 1$ particles result in crossing times of $\mathcal{O}(100\,\text{ns})$ and yield on the order of 400 hits across the detector at near vertical angles[2]. In contrast, the low electronics noise rates in the detector result in random noise hits, uncorrelated in space and time. The readout time window is sliced into sub-windows based on these temporal hit distributions. Spatial clustering is then performed to localize regions of correlated activity. After clustering is performed, each of the resulting activity candidates needs to have additional reconstruction algorithms applied to determine if the topological nature of the activity is consistent with low energy interactions or something else, such as an electromagnetic shower or a muon track. The standard NOvA event reconstruction algorithms are not well matched to this task due to the span of energies over which the identification is performed, ranging from the multi-GeV regime that dominates the cosmic ray flux seen by the detector, to the GeV-scale beam neutrino interactions for which the detector geometry was optimized, down to the tens of MeV level which characterizes the supernova neutrino energy spectrum. In particular, low energy interaction candidates are dominated by clusters with multiplicities insufficient to form a track or shower in the reconstruction algorithms used for oscillation analyses. A typical NuMI beam neutrino interaction produces tens of hits, so these algorithms generally require a minimum of 4–10 hits distributed across many detector planes with no more than a few gaps. Low energy interaction reconstruction instead relies on hit density and proximity, and does not place a minimum hit requirement on the candidate cluster. Thus, candidates for low energy interaction reconstruction are taken as those hit clusters remaining after higher energy processes are filtered out.

The supernova signal IBD interactions are expected to have visible energy signatures in the tens of MeV based on their parent neutrinos' spectrum. The NOvA detector's cellular geometry and 63% active fraction result in an approximate energy deposition of 8–10 MeV per cell crossed by the IBD positron. At these expected energy deposition rates, the upper tail of the neutrino energy spectrum is expected to produce hit clusters which extend between 1–4 cells (6–26 cm) corresponding to energies up to 40 MeV. Individual channels have a lower threshold for hit detection that is tuned to suppress noise from the electronics. This suppression threshold corresponds to the equivalent light output of approximately 71% of the average response of a minimum ionizing particle passing through the far end of a detection cell. This results in a worst-case detection threshold of approximately 8 MeV for interactions near the bottom and east edges of the detector, at the opposite ends of the cells from where the front-end readout boards are located.

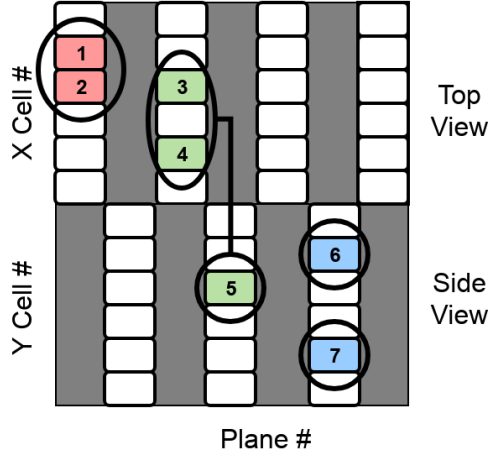[2]The NOvA Far Detector contains 384 cells per plane.

Figure 5. Illustration of cluster finding procedure for 7 example hits (numbered). Hits 1 and 2 will form a cluster only in the X-view. Hits 3, 4, and 5 will form a cluster in both X- and Y- views (this cluster can be considered a neutrino interaction candidate). Hits 6 and 7 will not be connected to any group, as they are too far apart. The Z-axis is left-to-right in this figure.

The neutrino interactions expected from a supernova thus produce very small clusters containing only a few hits. Any such clusters of hits are potential neutrino interaction candidates, and are reconstructed as described in the following sections.

3.2.1   Position selection

Hits belonging to the same cluster must be separated by not more than one cell within the same plane and contain cells from neighboring scintillator planes, meaning that they must contain cells of different orientation (X and Y). Clusters with only hits in cells on the same plane (X and X, or Y and Y) are not considered in this analysis, as lack of a 3D position prevents the next step (time correction). Figure 5 illustrates the selection of the clustering algorithm.

3.2.2   Time correction

The NOvA detectors' front-end readout systems are fully synchronized and have corrections applied at the hardware level for signal propagation delays within the timing and clock systems. However, these corrections do not include corrections for the signal propagation between the daisy-chained timing links that connect the Data Concentrator Modules (DCMs) that are physically positioned on the top and side faces of the detectors. These propagation delays have been measured for each of the DCM positions, and range from 15–120 ns corresponding to the near and far sides of the readout chain. These timing corrections are applied in the software layer of the supernova trigger to the raw timestamps read out for each of the hits in the detector in order to properly match scintillation signals produced in different cells across the detector. These corrections are the known time shifts in the detector synchronization chain [24] and the propagation delay resulting from the scintillation light being transported along the wavelength shifting fiber optic path to the APD readout at the end of the detection cell (Fig. 6). The correction algorithm takes into account the delay for the light transportation in the fibers, using the fiber length and measured index of refraction. The algorithm assumes an origination point for the light to correspond to the intersection of the X and Y hits in the
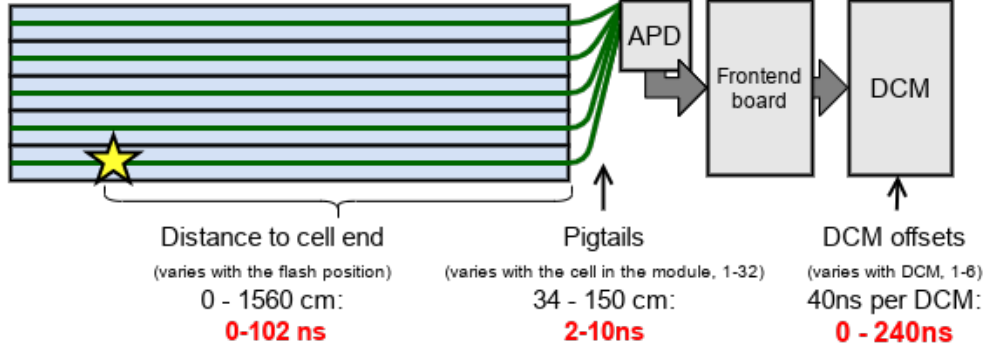
Figure 6. Timing corrections applied to the scintillation hit: starting with the light propagation time through the cells, then through optical fiber pigtails, into a unit of the front-end electronics and finally to the Data Concentrator Module ("DCM").

candidate cluster, and computes the distance to the corresponding APD readouts for X-view and Y-view planes. The application of this correction restricts the analysis to considering only clusters containing both X and Y hits. Since X-Y pairs are already required to reduce the accidentals rate from correlated noise in the electronics, this correction does not result in an additional degradation of the signal detection efficiency.

The single-hit timing resolution of the NOvA near and far detectors has been measured both in situ using cosmic ray muon tracks and in a dedicated teststand which was used to precisely characterize the front-end amplifier and shaper response functions that are needed for the calculation. These measurements result in a single-hit timing resolution function which depends on the photo response of the cell. This results in an expected timing resolution of 12 ns at a 200 ADC signal level, and less than 8 ns above 400 ADC. This resolution is used to set the timing coincidence level for the hit matching at 32 ns, corresponding to an envelope allowing for approximate fluctuations of $2.0\,\sigma$ for the lowest light response levels.

3.3 Candidate selection

The siting of the NOvA Far Detector on the surface under a 3.6 mwe overburden results in a significant flux of cosmic ray induced activity in the active volume of the detector. In particular, this flux includes electromagnetic shower activity which originates from interactions in the overburden of the detector hall and can mimic the low energy interaction topology. To reject this background source, a fiducial volume cut is applied to the data. This cut rejects activity coming from particle and shower penetration into the detector volume. The fiducial region has a boundary of 16 cell widths (62 cm), corresponding to 1.5 radiation lengths in both the X-view and Y-view from the bottom and sides of the detector. The boundary is set to 24 cell widths (94 cm), corresponding to 2.4 radiation lengths from the top face of the detector to provide additional attenuation of electromagnetic activity and to reduce the contamination of the signal from neutrals penetrating deep into the detector prior to interaction. For the Near Detector, the cut is 8 cells for X and Y and 8 planes for Z.

Finally, we apply a cut on the total ADC value of all hits in the cluster (Fig. 7). A range of acceptable ADC values was chosen to maximize the ratio of signal to the average background fluctuation $N_{sg}/\sqrt{N_{bg}}$, eliminating low energy noise hits and higher energy cosmogenic remnants. Table 3 summarizes the ADC and fiducial volume cuts applied to each cluster to be considered a neutrino candidate.
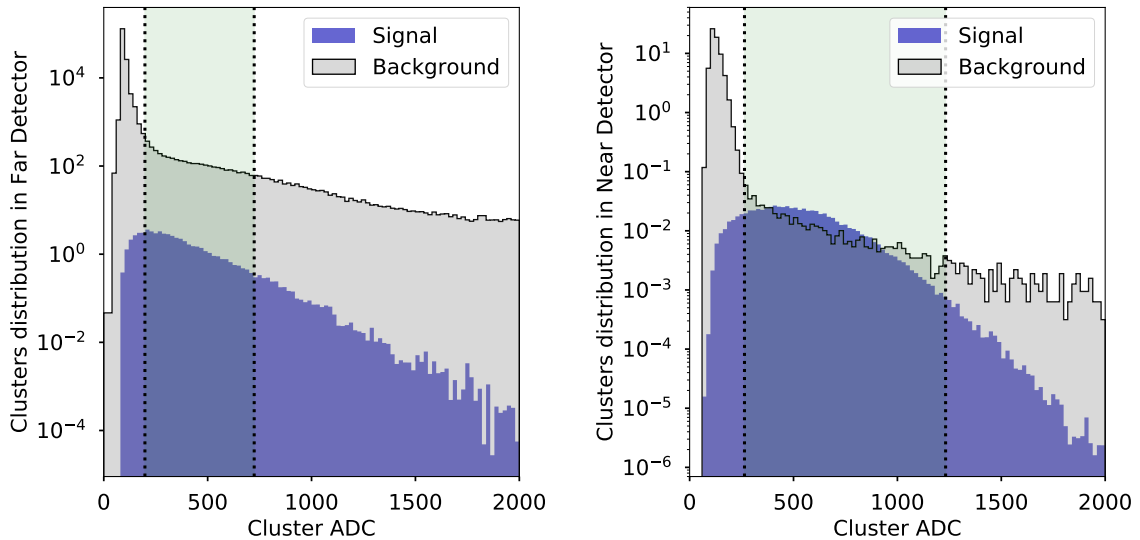
Figure 7. Selected ADC range for candidate clusters for the Far Detector (left) and Near Detector (right). The signal clusters are from the Monte Carlo simulation of $9.6\,\mathrm{M_\odot}$ supernova at $10\,\mathrm{kpc}$ distance and the background clusters are from minimum bias data. The range between the vertical dotted lines shows the ADC cut (from Tab 3) used to select the best $N_{sg}/\sqrt{N_{bg}}$ ratio for inclusion in the time series shown in Fig. 8.

Table 3. The selection criteria cuts for neutrino interaction candidates which were tuned as shown in Fig. 7 and Sec. 3.3.

Cut	Near Detector	Far Detector
ADC range	$[280, 1430]$	$[230, 910]$
Fiducial volume	$8 \leqslant \mathrm{X\ cell} \leqslant 88$ $8 \leqslant \mathrm{Y\ cell} \leqslant 88$ $8 \leqslant \mathrm{Z\ plane} \leqslant 184$	$16 \leqslant \mathrm{X\ cell} \leqslant 368$ $16 \leqslant \mathrm{Y\ cell} \leqslant 360$ $8 \leqslant \mathrm{Z\ plane} \leqslant 888$

3.4 Removing time-correlated candidate groups

After the background rejection procedures described above, there remains some rate of non-neutrino candidates produced by electromagnetic showers induced by the cosmic rays in the detector. The neutrino interactions from supernovae should not be correlated on short timescales, so we reject any pair of interaction candidates with timestamps closer than $250\,\mathrm{ns}$. Since the number of candidates at this step is low, this rejection produces a dead time less than 0.15%. This rejection significantly decreases the variation of the background candidates in time (Fig. 8) so that the background level follows a Poisson distribution.

3.5 Selection results

Applying the described selection procedure, we can estimate the detection efficiency using a simulated sample of positrons uniformly distributed within the detector and with random directions. This allows the calculation of the efficiency of detecting an individual positron as a function of positron energy, as shown in Fig. 9. This produces a signal to noise ratio
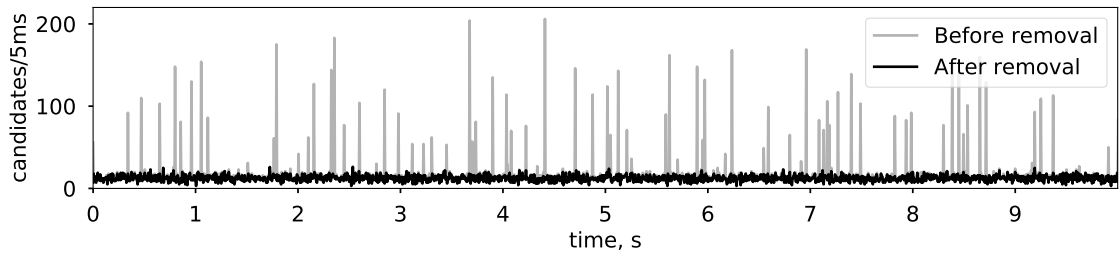
Figure 8. A time series of potential SN neutrino candidates seen at the Far Detector. Supernova neutrinos would be scattered randomly in time while remnants of electromagnetic interactions are correlated in time and appear in the form of peaks (grey). This background can easily be removed by cutting out the peaks (see Sec. 3.4 for details), causing 0.15% deadtime.

Table 4. The absolute survival efficiencies for each selection cut that is applied in the trigger algorithms. Survival fractions are computed independently for each cut as applied to both background activity in the detector and neutrino signal corresponding to the first second of a $9.6\,\mathrm{M}_\odot$ supernova at $10\,\mathrm{kpc}$. The aggregate efficiency of all cuts is also computed.

	Cut	Background		Signal	
		N_{bg}/s	ε	N_{sg}/s	ε
Far Detector	Reconstructed clusters	322811.99	100.00%	316.24	100.00%
	X and Y hits	231866.53	71.83%	145.16	45.90%
	$N_{hits} \leqslant 4$	310010.78	96.03%	315.06	99.63%
	Fiducial Volume	172281.67	53.37%	118.45	37.46%
	ADC cut	25879.67	8.02%	216.38	68.42%
	Total	2483.21	0.77%	86.64	27.40%
Near Detector	Reconstructed clusters	403.95	100.00%	3.16	100.00%
	X and Y hits	215.64	53.38%	2.19	69.35%
	$N_{hits} \leqslant 4$	394.81	97.74%	3.15	99.67%
	Fiducial Volume	68.10	16.86%	1.49	47.23%
	ADC cut	24.30	6.02%	2.73	86.29%
	Total	0.52	0.13%	1.28	40.43%

of 1:29 at the FD and 2.5:1 at the ND for a simulated $9.6\,\mathrm{M}_\odot$ supernova at $10\,\mathrm{kpc}$. Table 4 summarizes the candidate selection cuts and their effect on the number of candidates during the first second of a supernova.

At this stage, most of the obvious non-SN related candidates have been removed. The count of remaining candidate neutrinos is passed to the time series discussed in Sec. 5.

4 Trigger system for supernova detection

4.1 Data-driven triggering in NOvA

NOvA's Data-Driven Trigger (DDT) system, described in Sec. 1.1, is used to perform fast data reconstruction online in order to decide which time ranges of data should be saved for further offline analyses. To achieve this, the data stream from the detector is sliced into $5\,\mathrm{ms}$ chunks
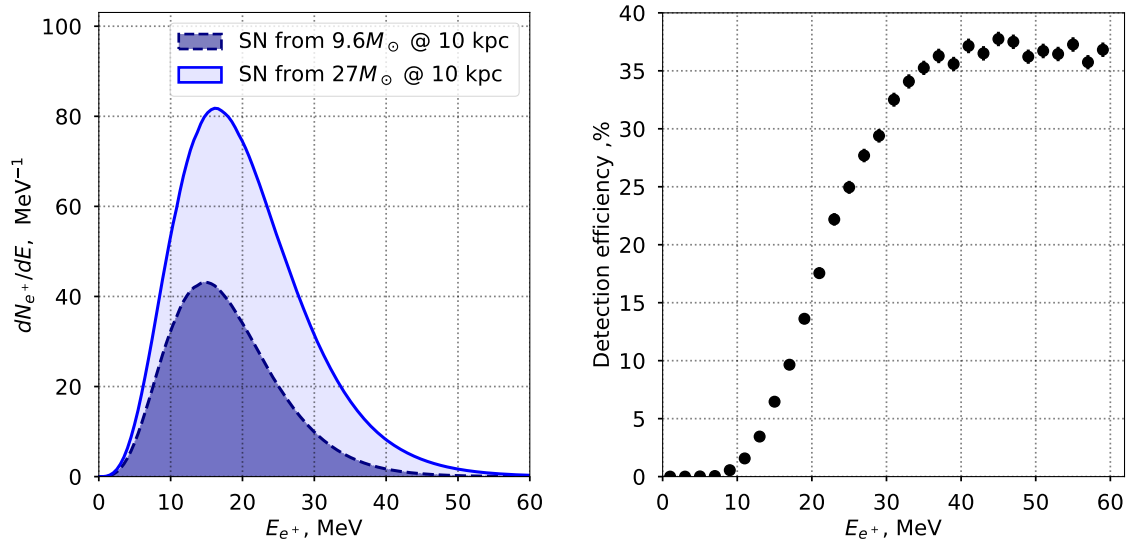
Figure 9. Positron spectrum from simulated supernova neutrino IBD interactions in the Far Detector (left) and efficiency of positron detection as a function of positron energy (right) with the cuts summarized in Tab. 4.

(called "milliblocks") and, for supernova detection, data in these milliblocks are subjected to the selection criteria described in Sec. 3 to count the number of potential supernova neutrino candidates in each 5 ms.

4.2 Supernova trigger infrastructure

In contrast to other NOvA triggers for which the trigger decision is made based on one 5 ms milliblock of data, the neutrino signal from a nearby supernova would last for tens of seconds. It would also likely not be evident in any single milliblock, given the comparatively low signal to noise ratio seen in Fig. 7. Thus, the accumulated information from hundreds of milliblocks must be used to decide if a supernova has been observed by the NOvA detectors. This must happen in parallel, as consecutive milliblocks of time are stored on different physical buffer node computers, with the resulting statistics being reported back to a central process on the "global trigger" node of the DAQ.

Thirteen processes on any given buffer node computer are running an instance of the analysis chain described above on a milliblock of data resident in the computer's memory, using eleven of the node's sixteen cores. This results in a count of potential positron candidates in that block of data, which the process reports to the central global trigger manager node. This node sorts these counts into a consecutive time series, in the same way all the other milliblocks of data are counted by many such processes through the DAQ server farm. This time sequence is convolved with the filtering kernel described in Sec. 5 to suppress background fluctuations and enhance the statistical significance of any potential signal. Should data be found that are consistent with a burst of positrons from IBD interactions of supernova electron anti-neutrinos, the global trigger issues a trigger request to the system, and the relevant time block is saved to disk. A total of 45 s of data is saved, starting 5 s before the triggered time to record a baseline of data before the neutrinos arrived.

4.3 Triggering delay

One of the main characteristics of the triggering system is a reaction time: the delay between the time when the neutrino signal from the supernova explosion reaches the detector and the moment when the trigger message would be issued. When the data is being buffered, too long a delay could result in a trigger issued after the data to be saved have fallen out of the buffer. Additionally, it is desirable to issue as prompt an alert to SNEWS as possible. This reaction time is defined by the individual delays in the supernova trigger pipeline.

We describe the sources of these delays and their average values for the Far Detector. First, the DAQ system must read out detector channels, build the milliblock data slice, and deploy it to one of the $\sim$2200 parallel DDT processes, which takes 3.5 s on average. The DDT processes perform the background subtraction and reconstruction of neutrino interaction candidates as described above. This processing takes about 5 s for one milliblock.

Before sending the calculated neutrino candidate rate, the buffer node accumulates ten measurements to form a packed message to send. This is done to reduce the load on the network traffic between the buffer nodes and the global trigger node. Accumulating ten milliblocks on one buffer node takes, on average, 8.5 s.

The messages with candidate rates and milliblock timestamps arrive to the global trigger from parallel DDT processes unsorted in time, so additional delay arises from buffering incoming data until a continuous one second of data is populated. This delay varies depending on the time spread of incoming messages. An average value for this delay is 18 s.

Finally, the global trigger needs to process at least 5 s of continuous data to decide if it contains a supernova signal.

In case any data point is lost (*e.g.* a milliblock was not processed or data was corrupt), the system waits for its arrival for up to 60 s before skipping this point in the processing. This defines the maximal possible delay.

In the case of the Near Detector, most of the delays for processing and waiting for the data are negligible, because the data flow is much smaller and so the number of parallel processes is reduced to 169.

The trigger system delay was measured as the difference between the milliblock timestamp and the time when it reaches the end of the system pipeline. The total delay for the Far Detector is 40 s on average and 60 s at maximum. The delay for the Near Detector is very stable at the level of 5.7 s. These latencies are sufficiently low to provide a useful supernova trigger: both are much less than the buffer depth, and are among the lowest of any of the SNEWS experiments.

4.4 Cross-detector triggering

NOvA is composed of two detectors both of which are sensitive to SN neutrinos. Once one of the detectors identifies a potential supernova burst, a trigger is sent to the other detector to ensure that data is also saved there. This cross trigger results in a logical "OR" of the individual triggers of the NOvA near and far detectors when calculating the trigger sensitivities.

Future work is planned to combine the time series acquired at each detector. Combining the two series will result in better rejection of fluctuations and more sensitivity to a real signal.

4.5 External supernova trigger from SNEWS

To increase the chance that neutrinos from a galactic supernova would not be missed, the NOvA detectors will also save data based on an external trigger from the SNEWS coincidence network [5]. Should a coincidence between the supernova triggers of other neutrino experiments be made by the SNEWS project, an XML-RPC message is sent by the SNEWS server to the NOvA DAQ, triggering a 45 s readout of both NOvA detectors' data [25] starting 5 s before the SNEWS coincidence time. This connection is tested by saving a short ($50\,\mu$s) time window of data once per minute, and one full-length 45 s time block once per day at each detector.

To help reduce data processing bottlenecks at the event building stage in NOvA, each unit of data will be included in one supernova-related trigger at a time, rather than being included in multiple simultaneous triggers. For example, a real supernova would ideally produce self-triggers at each detector, as well as cross-triggers from each detector, and an alert from SNEWS. Any overlapping times from all these long readout windows will be saved only once per detector.

In the future, in addition to NOvA saving this data, these triggers will be reported to SNEWS to help form a prompt coincidence with other neutrino detectors around the world.

5 Trigger sensitivity

After the parallel DDT processes have performed searches for IBD interaction candidates, data on the candidate rate per 5 ms are sorted and accumulated in a time series $\{t_i, n_i\}$. In order to decide if this time series contains a signal from a supernova, we scan the incoming data and test the "background-only" ($H_0 = B$) and "signal + background" ($H_1 = B + S$) hypotheses. These hypotheses predict a Poisson distribution for the number of candidates in the i-th time bin, with mean values λ:

$$P(n_i|H_0) = \mathrm{Poisson}(n_i|\lambda = B),$$
$$P(n_i|H_1) = \mathrm{Poisson}(n_i|\lambda = B + S_i).$$

In order to discriminate these hypotheses based on the data in a time window $\vec{n} = \{n_i\}$, we construct the log likelihood ratio value

$$\ell(\vec{n}) \equiv \log \prod_i \frac{P(n_i|H_1)}{P(n_i|H_0)} = \sum_i n_i \cdot \log(1 + S_i/B) \tag{5.1}$$

and use it as a test statistic. Thus, our discrimination power depends on the average background level B and an expected signal profile $\vec{S} = \{S_i\}$. Such discrimination is optimal in case the measured signal $\vec{S'}$ coincides with the expected one $\vec{S}$. However, choosing $\vec{S}$ such that it follows the general features of the SN signal also gives results that do not drastically change sensitivity for two very different signal models (see section 5.1).

In order to decide if the observed signal contains evidence of a supernova neutrino burst, we calculate the p-value

$$p(\vec{n}) = P(\ell > \ell(\vec{n})|H_0),$$

and, finally, compute the signal significance score in "sigmas":

$$z(\vec{n}) = \mathrm{erf}^{-1}\left(1 - 2p(\vec{n})\right). \tag{5.2}$$

The significance score z for the "background-only" hypothesis H_0, follows standard normal distribution by construction:

$$P(z|H_0) = \mathcal{N}(z|\mu = 0, \sigma = 1).$$

If the significance score exceeds threshold $z_0 = 5.645\,\sigma$, the trigger signal is sent. This threshold corresponds to the average rate of one false trigger from background fluctuations per week, the target rate for SNEWS input.

During the trigger system operation the background level B is estimated at the end of every ten minutes period based on the activity in this period. Thus the triggering system can adapt to slow changes in background conditions, maintaining the same false alarm probability: this does not appreciably change the supernova sensitivity. Sudden background changes on timescales less than ten minutes can cause the false trigger alarms, as observed during the commissioning (see section 6). Large background changes are indicative of detector problems, and quickly fixed lest all of NOvA's analyses be degraded.

5.1 Results

Figure 10 shows an example of how the trigger system processes the input data time series of candidates per 5 ms time bin (n_i) where the counts in the top plot are potential neutrino candidate clusters drawn from actual minimum bias detector data (grey) with the addition of a simulated supernova signal (blue) at $t = 20\,\text{s}$. The next three plots are time series of the resulting significance scores $z(\vec{n})$ calculated using three types of expected signal shapes: a naive "top hat" shape; and two shapes drawn from models [13] of specific low-mass ($9.6\,\text{M}_\odot$) and high-mass ($27\,\text{M}_\odot$) progenitor stars. The shape which was drawn from the model which was injected in this test (the $9.6\,\text{M}_\odot$ model) has the highest significance as expected. However, both other models also match well enough to produce a SN trigger readout at the correct time.

To decide which shape template to use in the online trigger, the two supernova models were tested against each shape template for both detectors as a function of distance. Figures 11 and 12 show the signal significance for both supernova models vs. distance for each of the three shapes. The horizontal bands are significances corresponding to various "false alarm rates". The target rate of accidental triggers for SNEWS input is once per week. When the threshold is set at that level the intersection of the model's central and that threshold yields the distance sensitivity to a supernova exploding as per that model when searched for using that shape template. This distance is listed on each plot.

The operational trigger system uses the expected signal shape from the $9.6\,\text{M}_\odot$ model to make its decision, as it represents the most general features of the supernova neutrino signal. The choice of optimizing for the the dimmer (and likely more commonly occurring) $9.6\,\text{M}_\odot$ model is validated by the good performance obtained for both the $9.6\,\text{M}_\odot$ and the brighter $27\,\text{M}_\odot$ signal model, as shown in the middle plots in Figures 11 and 12.

No neutrino flavor changing oscillation effects were assumed when modeling the expected supernova neutrino flux. This "no-oscillation" methodology is used in the template simulations to separate model and parameter dependant features from the baseline templates of the trigger. To check for biases under this simplified assumption, we followed Ref. [26] to take into account simple adiabatic flavor conversion from MSW resonances in the stellar medium. This effect leads to a mixing, under the normal neutrino mass ordering hypothesis, or a swapping (under the inverted neutrino mass ordering, of $\bar{\nu}_e$ flux with $\bar{\nu}_x$ flux. The resulting $\bar{\nu}_e$ flux will have properties inherited from the $\bar{\nu}_x$ flux, resulting in fewer neutrinos but with
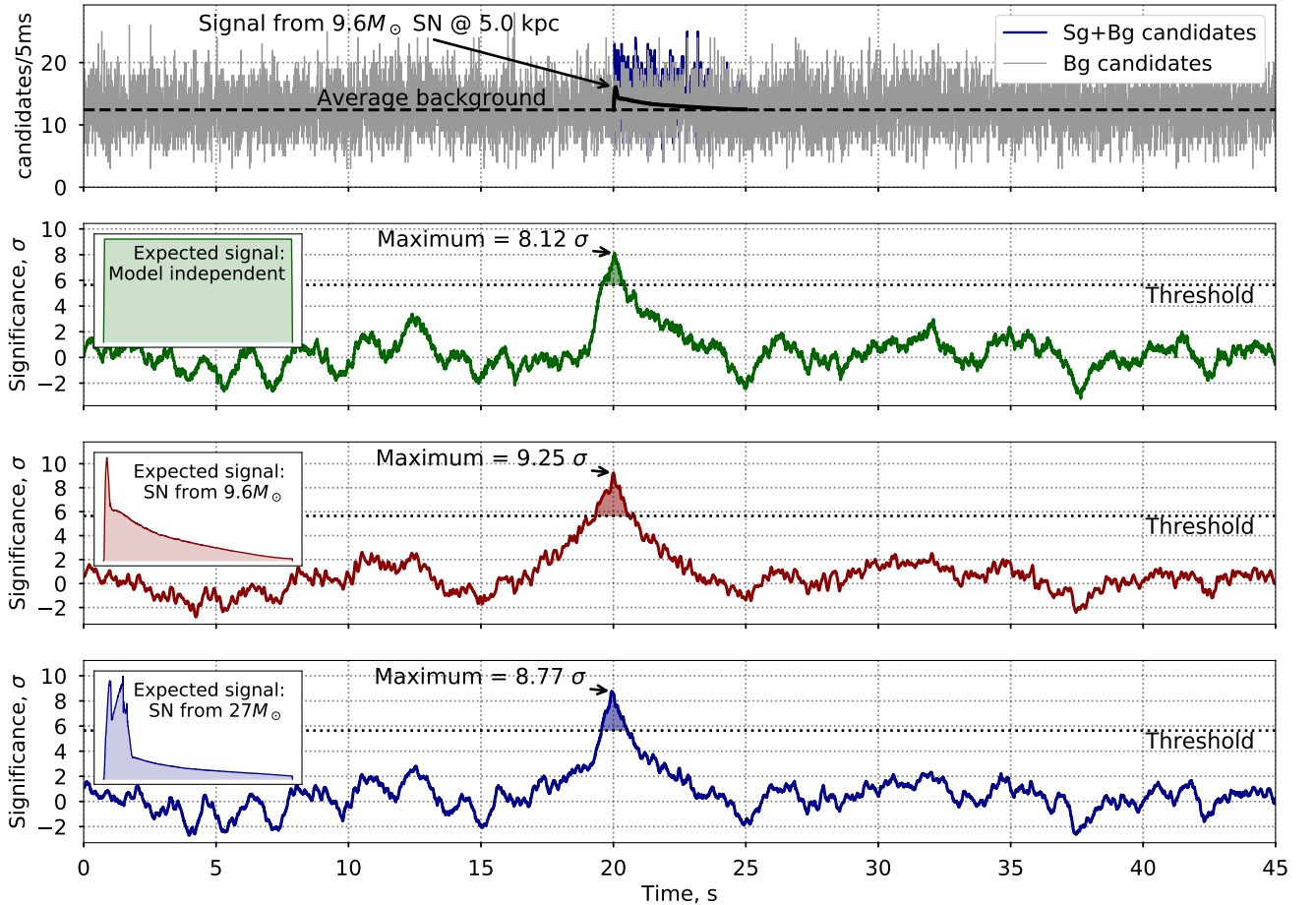
Figure 10. Example of the trigger system detecting a simulated supernova signal from a star 5 kpc away. The top time series of neutrino candidates per 5 ms bin in the NOvA Far Detector shows the location and size of an injected signal. The next three time series are the significances of the data matching the expected signal shape starting at that point in the time series, expressed as Gaussian sigmas, calculated as described in Sec. 5. The three signal shapes are: a uniform one second increase in rate (top pane); the detector response for a $9.6 \, M_\odot$ progenitor core-collapse model (middle pane); and for a $27 \, M_\odot$ progenitor at the bottom. The injected signal is drawn from the middle model, causing it to match the best: but the other two templates still pick up the correct time ($t = 20 \, \mathrm{s}$) with high significance. Models are from [13].

higher neutrino energies than in the initial spectrum. This results in a two-sided effect on the expected number of events to be detected by NOvA. It results in 5 % (17 %) fewer neutrino interaction candidates for the brighter $27 \, M_\odot$ progenitor model, and 12 % (40 %) more neutrino candidates for the $9.6 \, M_\odot$ progenitor in the case of normal (inverted) mass ordering. The enhancement of the signal for the smaller progenitor star is caused by the energy dependence of the interaction cross-section and the detection efficiency. By using the "no-oscillations" methodology as a triggering template, NOvA has chosen a conservative choice, which does not push the spectra to the two extremes as would be in the case of including oscillations. This approach minimizes triggering biases with respect to the as yet unknown neutrino mass hierarchy and range of progenitor masses.
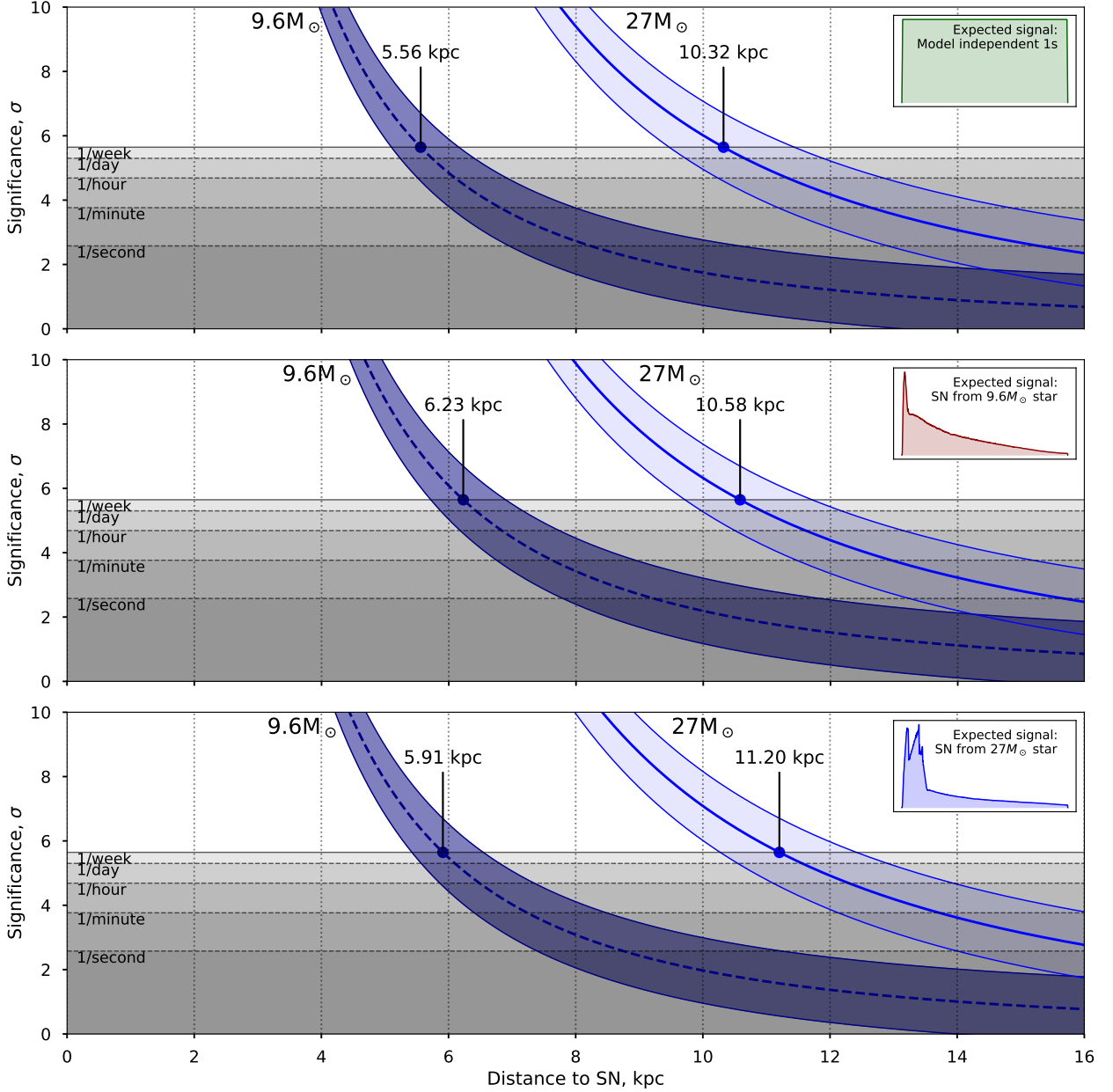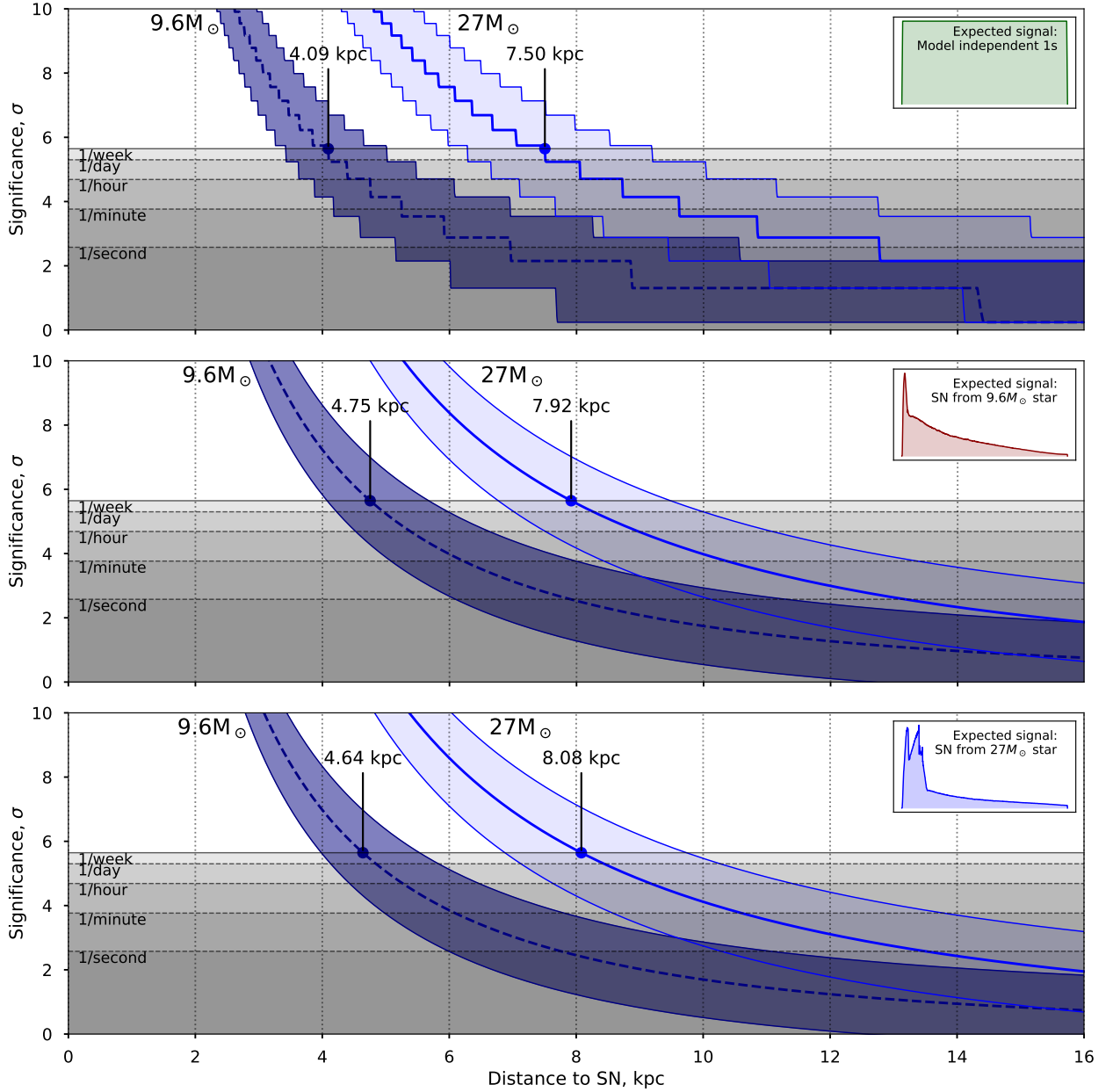
Figure 11. The expected significance of the supernova signal observations vs. the distance to the supernova for $9.6 \, \mathrm{M_\odot}$ and $27 \, \mathrm{M_\odot}$ progenitor stars in the Far Detector, compared to the rate of background induced triggers at various time scales (grey horizontal levels). The middle lines show the mean significance value, while the bands show the region with 68% significance distribution. The point at which the mean signal significance is equivalent to an accidental rate of once per week is noted in the plot, in kpc. The three signal shape templates used, from top to bottom, correspond to those shown in Fig. 10.

5.2   Probability of detecting the next galactic supernova

The probability of the NOvA detectors detecting a supernova for various distances (see Figs. 13 and 14) can now be convoluted with the observed spatial distribution of potential supernova progenitors from Ref. [27]. This integral allows the calculation of the probability

Figure 12. The expected significance of the supernova signal observations vs. the distance to the supernova for $9.6\,\mathrm{M_\odot}$ and $27\,\mathrm{M_\odot}$ progenitor stars in the Near Detector, compared to the rate of background induced triggers at various time scales (grey horizontal levels). The point at which the mean signal significance is equivalent to an accidental rate of once per week is noted in the plot, in kpc. The three signal shape templates used, from top to bottom, correspond to those shown in Fig. 10. The rate at the Near Detector is small, leading to discrete jumps in the top figure.

to detect the next galactic supernova with the NOvA supernova trigger system. We have a 22.6% and 49.2% chance to detect a supernova from $9.6\,\mathrm{M_\odot}$ and $27\,\mathrm{M_\odot}$ progenitor stars, respectively, assuming the same spatial distribution for both progenitor masses. (see Fig. 15).

Figure 13. NOvA's sensitivity to a galactic supernovae vs. distance by supernova model and expected signal shape for the Far Detector. The fraction of supernova occurrences for which the signal probability would be above threshold is plotted as a function of distance for the cases presented in Fig. 11.
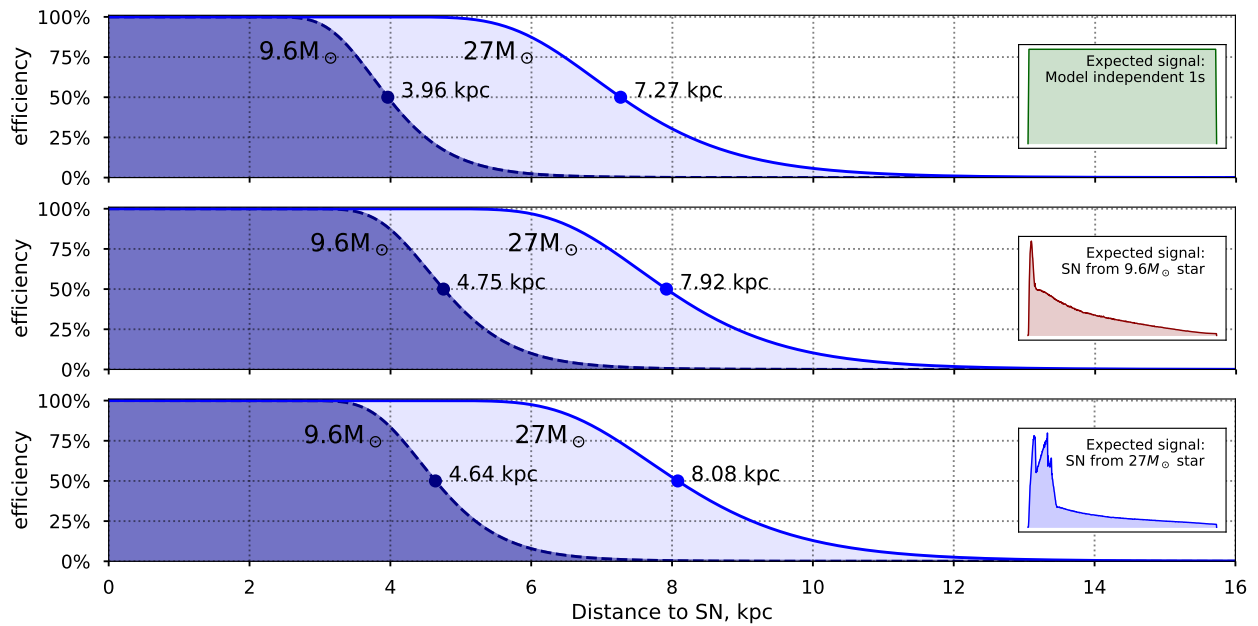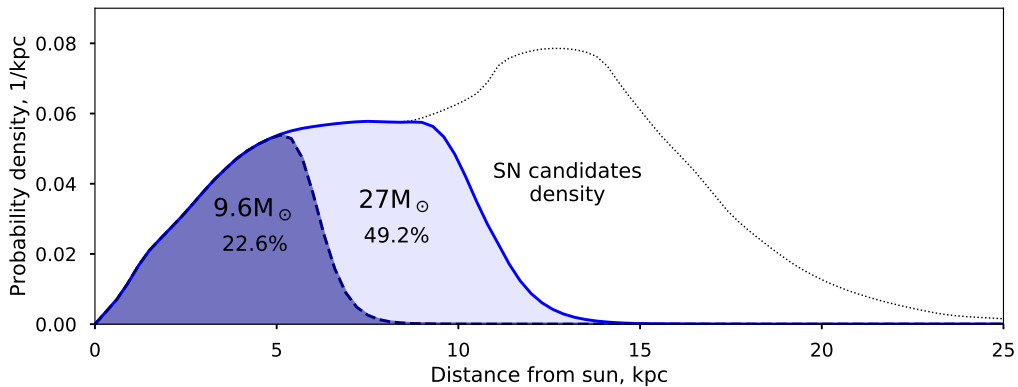

Figure 14. NOvA's sensitivity to a galactic supernova vs. distance by supernova model and expected signal shape for the Near Detector. The fraction of supernova occurrences for which the signal probability would be above threshold is plotted as a function of distance for the cases presented in Fig. 12.

Figure 15. The NOvA experiment's sensitivity to galactic supernova vs. distance. The dark blue area is for a $9.6\,\mathrm{M}_\odot$ progenitor, and the light blue area from a brighter $27\,\mathrm{M}_\odot$ star: both models are from [13]. The dotted curve for supernova progenitor density is from [27]. Percentage is the fraction of SN candidates covered by the trigger, for the two cases of progenitor masses.

6 Trigger system commissioning

Since deploying the supernova triggering system on November 1, 2017, several fixes and upgrades have been made to reduce the rate of false triggering caused by instabilities in the detector and readout conditions. During the 318 day commissioning period from October 1, 2018 to August 15, 2019, the NOvA Far Detector triggering system issued 71 supernova triggers. Each trigger requests the data readout within 45 s. In the case when another supernova trigger is received within the same 45 s window, the triggers are merged into one request for a longer readout. The time distribution of the issued triggers is shown in Fig. 16.

Out of the observed 71 supernova triggers, 24 were concentrated in three trigger bursts. These bursts were caused by readout instabilities, described below.

6.1 Partial detector data

It can take up to ten minutes after the detector run restarts for the readout electronics to fully synchronize, resulting in an underestimation of the background level by the supernova triggering system. After the readout is synchronized, the system is triggered by the perceived increase in detector activity. This false triggering mode is prevented by adding a filter to remove incomplete data from the trigger pipeline.

6.2 Noise channel map updates failure

As discussed in Sec. 3.1.3, a map of noisy electronic channels is updated every hour in order to adapt to changes in electronics conditions. When such an update is not performed (in case the computing process has stopped), a new noisy channel can emit a periodic burst of noise hits, causing a false trigger every ten minutes This problem was solved by setting up additional monitoring of the noise map updating process.

6.3 Triggering rate

The remaining 47 supernova triggers during the commissioning period are considered to be the result of the expected random background fluctuations. Their average rate of $1/(6.77\,\pm$
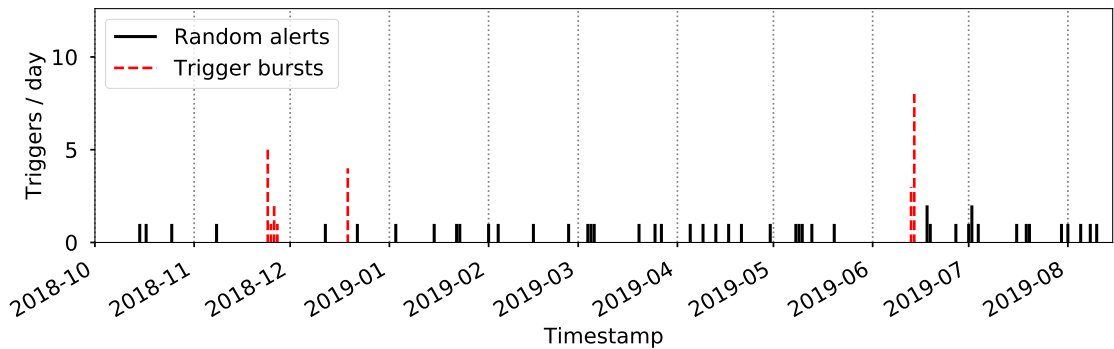
Figure 16. Time distribution of NOvA SN triggers issued by the system on the Far Detector during the commissioning period. Red dashed lines show trigger bursts associated with unstable detector or readout conditions as discussed in Sec. 6.
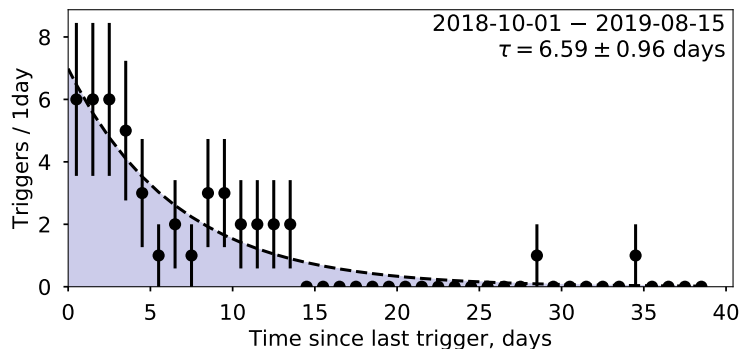

Figure 17. Distribution of the time intervals between subsequent SN triggers at the NOvA Far Detector (excluding those due to "bursts"). The dashed line shows the exponential fit of the distribution, with the time constant $\tau = 6.59 \pm 0.96$ days.

0.98 days) is in agreement with the expected one trigger per week. The distribution of time intervals between subsequent triggers, as shown in Fig. 17, is consistent with an exponential distribution with best fit average rate of $1/(6.59 \pm 0.96\,\text{days})$ (statistical errors).

7 Summary

The NOvA experiment's detectors are sensitive to the burst of neutrinos emitted by a core-collapse supernova in our galaxy through the detection of low energy ($\mathcal{O}(10\,\text{MeV})$) positrons from inverse beta decay interactions. The time structure and rate excess of these interactions allow for the ensemble of interactions to be distinguished from other cosmogenic backgrounds in the NOvA detectors. The NOvA Near and Far detectors have different signal to noise ratios for these signatures due to the size of their overburdens and effective detector masses. For both near and far detectors, data from the detectors are buffered by the DAQ systems and the data is reconstructed in near real time through low latency pattern recognition and background subtraction algorithms. The rate of supernova neutrino-like events is assembled into a time series. The time series is compared to template distributions from simulated supernovae to determine a likelihood metric which is used to compute the significance of the

time series having originated from a supernova. When the significance exceeds a threshold set within the trigger system, a trigger signal is generated which causes the DAQ system to initiate the recording of a 45 s time window around the region of interest. This region captures the supernova neutrino burst and activity both prior and subsequent to it, where the intervals are intended to yield a pre-sideband and a trailing tail that can extend out to black hole formation.

The significance threshold for this trigger process has been set to balance the trigger efficiency for detection of a supernova event with the false positive rate resulting from Poisson variation in the detector's activity. Under these conditions, the NOvA supernova trigger is estimated from Monte Carlo modeling of supernova neutrino spectra to achieve a 50% or higher trigger detection efficiency for a $9.6\,M_\odot$ progenitor's collapse out to a distance of $6.2\,\text{kpc}$. Similarly, the detectors achieve a 50% or higher trigger detection efficiency for a brighter $27\,M_\odot$ progenitor out to a distance of $10.6\,\text{kpc}$. The resulting supernova system triggered 71 times between Oct. 1, 2018 and Aug. 15, 2019 with an average rate of $1/(6.59\pm 0.96\,\text{days})$. During this period, there has been neither an optical observation nor a neutrino based observation from other experiments of a Milky Way supernova that is coincident with these triggered events. We have found the triggering rate to be consistent with expected statistical fluctuations in the detector backgrounds and with periods of known instability in the detector readouts.

At distances greater than $10\,\text{kpc}$, NOvA relies primarily on capturing a supernova neutrino burst through the use of an external trigger signal from the SNEWS coincidence network. Future work on combining the time series obtained from both the near and far detectors into a joint significance will allow for greater sensitivity and reach for the self-triggering system.

Acknowledgments

References

[1] R. M. Bionta et al., *Observation of a neutrino burst in coincidence with supernova SN1987A in the Large Magellanic Cloud*, Phys. Rev. Lett. **58** (1987) 1494.

[2] KAMIOKANDE-II collaboration, *Observation of a neutrino burst from the supernova SN1987A*, Phys. Rev. Lett. **58** (1987) 1490.

[3] E. N. Alekseev, L. N. Alekseeva, V. I. Volchenko and I. V. Krivosheina, *Possible detection of a neutrino signal on 23 February 1987 at the Baksan underground scintillation telescope of the Institute of Nuclear Research*, JETP Lett. **45** (1987) 589.

[4] M. Aglietta et al., *On the event observed in the Mont Blanc underground neutrino observatory during the occurrence of Supernova 1987a*, Europhys. Lett. **3** (1987) 1315.

[5] P. Antonioli et al., *SNEWS: The Supernova Early Warning System*, New J. Phys. **6** (2004) 114 [astro-ph/0406214].

[6] NOvA collaboration, *The NOvA Technical Design Report*, .

[7] P. Adamson et al., *The NuMI Neutrino Beam*, Nucl. Instrum. Meth. **A806** (2016) 279 [1507.06690].

[8] R. L. Talaga, J. J. Grudzinski, S. Phan-Budd, A. Pla-Dalmau, J. E. Fagan, C. Grozis et al., *PVC Extrusion Development and Production for the NOvA Neutrino Experiment*, Nucl. Instrum. Meth. **A861** (2017) 77 [1601.00908].

[9] S. Mufson et al., *Liquid Scintillator Production for the NOvA Experiment*, Nucl. Instrum. Meth. **A799** (2015) 1 [1504.04035].

[10] A. Norman et al., *Performance of the NOvA Data Acquisition and Trigger Systems for the full 14 kT Far Detector*, J. Phys. Conf. Ser. **664** (2015) 082041.

[11] K. Scholberg, *Supernova Neutrino Detection*, Ann. Rev. Nucl. Part. Sci. **62** (2012) 81 [1205.6003].

[12] T. Totani, K. Sato, H. E. Dalhed and J. R. Wilson, *Future detection of supernova neutrino burst and explosion mechanism*, The Astrophysical Journal **496** (1998) 216.

[13] A. Mirizzi, I. Tamborra, H.-T. Janka, N. Saviano, K. Scholberg, R. Bollig et al., *Supernova Neutrinos: Production, Oscillations and Detection*, Riv. Nuovo Cim. **39** (2016) 1 [1508.00785].

[14] K. Nakazato, K. Sumiyoshi, H. Suzuki, T. Totani, H. Umeda and S. Yamada, *Supernova neutrino light curves and spectra for various progenitor stars: From core colllapse to proto-neutron star cooling*, The Astrophysical Journal Supplement Series **205** (2013) 2.

[15] A. Strumia and F. Vissani, *Precise quasi-elastic neutrino/nucleon cross-section*, Physics Letters B **564** (2003) 42 .

[16] W. J. Marciano and Z. Parsa, *Neutrino–electron scattering theory*, Journal of Physics G: Nuclear and Particle Physics **29** (2003) 2629.

[17] B. Armbruster, I. Blair, B. Bodmann, N. Booth, G. Drexlin, V. Eberhard et al., *Measurement of the weak neutral current excitation $^{12}C(\nu_\mu, \nu'_\mu)^{12}C^*(1^+, 1; 15.1\, MeV)$ at $E_{\nu_\mu} = 29.8\, MeV$*, Physics Letters B **423** (1998) 15 .

[18] C. Andreopoulos, A. Bell, D. Bhattacharya, F. Cavanna, J. Dobson, S. Dytman et al., *The GENIE neutrino Monte Carlo generator*, Nuclear Instruments and Methods in Physics Research Section A: Accelerators, Spectrometers, Detectors and Associated Equipment **614** (2010) 87 .

[19] S. Agostinelli et al., *Geant4 — a simulation toolkit*, Nuclear Instruments and Methods in Physics Research Section A: Accelerators, Spectrometers, Detectors and Associated Equipment **506** (2003) 250 .

[20] A. Aurisano, C. Backhouse, R. Hatcher, N. Mayer, J. Musser, R. Patterson et al., *The NOvA simulation chain*, *Journal of Physics: Conference Series* **664** (2015) 072002.

[21] NOvA collaboration, *New Constraints on Oscillation Parameters from ν_e Appearance and ν_μ Disappearance in the NOvA Experiment*, *Phys. Rev.* **D98** (2018) 032012 [1806.00096].

[22] NOvA collaboration, *First measurement of muon-neutrino disappearance in NOvA*, *Phys. Rev.* **D93** (2016) 051104 [1601.05037].

[23] M. Baird, J. Bian, M. Messier, E. Niner, D. Rocco and K. Sachdev, *Event reconstruction techniques in NOvA*, *Journal of Physics: Conference Series* **664** (2015) 072035.

[24] NOvA collaboration, *The NOvA Timing System: A System for Synchronizing a Long Baseline Neutrino Experiment*, *J. Phys. Conf. Ser.* **396** (2012) 012034.

[25] A. Habig and J. Zirnstein, *Integration of the Super Nova Early Warning System with the NOvA trigger*, *Journal of Physics: Conference Series* **664** (2015) 082015.

[26] K. Scholberg, *Supernova Signatures of Neutrino Mass Ordering*, *J. Phys. G* **45** (2018) 014002 [1707.06384].

[27] A. Mirizzi, G. G. Raffelt and P. Serpico, *Earth matter effects in supernova neutrinos: Optimal detector locations*, *JCAP* **0605** (2006) 012 [astro-ph/0604300].